Title

Influence of soil-structure interaction on performance of a super tall building using a new eddy-current tuned mass damper

Journal

Structural Design of Tall and Special Buildings, 27(14)

ISSN

1541-7794

Authors

Zhou, Z
Wei, X
Lu, Z
et al.

Publication Date

2018-10-10

DOI

10.1002/tal.1501

Peer reviewed

Influence of soil-structure interaction on performance of a super tall building using a new eddy-current tuned mass damper

Zhiguang Zhou[1,2] | Xiaodong Wei[2] | Zheng Lu[1,2] | Boris Jeremic[3]

[1] State Key Laboratory of Disaster Reduction in Civil Engineering, Tongji University, Shanghai 200092, China [2]Research Institute of Structural Engineering and Disaster Reduction, Tongji University, Shanghai 200092, China 3Department of Civil and Environmental Engineering, University of California, Davis, California 95616, USA

Correspondence Zheng Lu, State Key Laboratory of Disaster Reduction in Civil Engineering, Tongji University, Shanghai 200092, China. Email: luzheng111@tongji.edu.cn

Summary

Tuned mass dampers (TMDs) can be used as vibration control devices to improve the vibration performance of high-rise buildings. The Shanghai Tower (SHT) is a 632-m high landmark building in China, featuring a new eddy-current TMD. Special protective mechanisms have been adopted to prevent excessively large amplitude of the TMD under extreme wind or earthquake loading scenarios. This paper presents a methodology for simulating behavior of the new eddy-current TMD that features displacement-dependent damping behavior. The TMD model was built into the SHT finite element model to perform frequency analysis and detailed response analyses under wind and earthquake loads. Furthermore, soil-structure interaction (SSI) effects on wind and seismic load responses of the SHT model were investigated, as SSI has a significant impact on the vibration performance of high-rise buildings. It was found that SSI has more significant effects on acceleration response for wind loads with a short return period than for wind loads with a long return period. Some of the acceleration responses with SSI effects exceed design limits of human comfort for wind loads with shorter return periods. As to the seismic analyses, it was found that SSI slightly reduces the displacement amplitude, the damping force, and the impact force of the TMD.

1 INTRODUCTION

The design of high-rise buildings is typically controlled by wind and seismic loads. Although strength is important to consider, human comfort to wind and earthquake induced vibrations is in general the most important evaluation criterion. These vibrations could be controlled by introducing a tuned mass damper (TMD). A TMD is a device mounted within a structure to reduce the amplitude of vibrations.[1] The damping of a TMD is usually provided by a dashpot, often a conventional fluid viscous damper.[2] However, traditional viscous dampers may have the drawbacks[3]: limited service life, viscous property sensitive to heat generated by energy dissipation, and undesired flexibility and complexity in connections. To overcome these limitations, a new eddy-current TMD with additional permanent magnet and

conductor plate was used in SHT.[4] Based on *Faraday's Law of Induction*[5] and *Lenz's Law*,[6]eddy currents generated by moving a permanent magnet near a conductor will generate forces that oppose relative motion between the magnet and the conductor. Effects of those two physics laws, as described above, could be applied to TMD devices. The generated drag forces can be used to provide the damping force.

However, many buildings with TMDs are usually designed without considering the SSI effect. This might be acceptable sometimes for low-rise buildings on moderate soils or hard rocks.[7, 8] Nevertheless, for super tall buildings on soft soils such as soils in Shanghai, the effect of SSI may not be neglected. A TMD is effective only when the period of the TMD is very close to the nature period of the structure. The performance and effectiveness of a TMD device are reduced as the period of the TMD deviates away from the natural period of the structure. Wu et al.[9] concluded that when soil is very soft, TMD cannot effectively reduce the seismic response of the soil-structure system. On the other hand, when soil is moderately stiff, TMD should be tuned to the natural period of the soil-structure system instead of the fixed-based structure, in order to optimize the seismic performance of TMD.

As to the studies on SSI, Wolf[10] developed a method to perform an SSI analysis by using spring, mass, and dampers. Chatzigogos et al. presented a new formulation for modeling of shallow foundations of structures using the concept of macroelement.[11] By using the above methods, Moghaddasi et al.[12-14] used robust Monte Carlo simulation to analyze the SSI effects. Finn et al.[15] compared various numerical methods used in practice for simulating SSI effects. Venanzi et al.[16] pointed out that fixed-based assumption might not always be on the safe side. By studying buildings with different heights and different types of soils under wind load, Chen et al.[17-19] concluded that total displacement response of the structure considering SSI is always greater than that without considering SSI and that this phenomenon becomes more significant if the building is high. Liu[20] developed a mathematical model for predicting wind-induced oscillations of a high-rise building with a TMD when SSI is considered and concluded that TMD more effectively suppresses structural vibrations for buildings with rigid foundations and that SSI needs to be considered for buildings with soft foundations. Li et al.[21] studied the influence of SSI on the collapse resistance capacity and failure sequences of the SHT model without a TMD.

In this paper, a method is presented for simulation of the new eddy-current TMD that shows displacement-dependent damping behavior. First, a stand-alone TMD model is developed to examine its dynamic characteristics. Then, the TMD model is embedded into the SHT model to perform analysis of response frequencies and for detailed analyses under loads from wind and earthquake. Furthermore, soil-structure interaction (SSI) effects for wind and seismic response of the SHT model are investigated.

2 OVERVIEW OF THE SHT

SHT is a super high-rise building with a height of 632 m, with a steel-concrete hybrid mega frame-core tube-outrigger structural system. The SHT is located in Lujiazui Financial Zone in Shanghai, China. The building has 127 floors above the ground and five floors below the ground level. It covers an area of 30,368 m^2, and the above ground floor area is 410,000 m^2, whereas the underground floor area is 168,000 m^2. The building includes nine zones in vertical direction, divided by eight strengthened stories with outriggers and belt truss. A photograph of SHT is shown in Figure 1.

Figure 1

Photograph of Shanghai Tower

Shanghai is a coastal city and may be hit by a severe typhoon. Due to the extreme height and long natural period of SHT, the wind-induced

acceleration response of the upper part of SHT might exceed the human comfort limit. According to the design of SHT, the maximum acceleration of building should not exceed 0.036 and 0.25 m/s^2 for wind load with 1- and 10-year return period, respectively. In addition, SHT is located in an area with a seismic intensity of seven-degree according to Chinese code. Therefore, earthquake and wind loading effects need to be considered. After a series of studies, a new eddy-current TMD was developed to control vibration response due to wind and earthquake excitations.

3 MODELING OF THE EDDY-CURRENT TMD

3.1 Overview of the TMD

A 1,000-ton eddy-current TMD was installed on the 125th floor of SHT. As illustrated in Figure 2(a), the mass block is suspended by four sets of cables that are 20.6 m long. A special protective system was incorporated to prevent excessively large amplitude motions of the TMD under extreme wind or earthquake scenarios. The protection system is composed of a snubber, a restraining ring, and eight viscous dampers. The snubber is fixed at the bottom of TMD. The restraining ring is connected to the 125th floor by the eight viscous dampers. The radius of the snubber is 0.5 m, and the radius of the restraining ring is 2 m. Thus, when the TMD amplitude exceeds 1.5 m, the snubber would impact the ring and the mass block movement would be restricted by the ring and the viscous dampers. The designed maximum displacement of the viscous dampers is 0.5 m. Thus, the maximum allowable relative displacement between 125th floor and TMD is 2 m, and the maximum allowable relative displacement between TMD and the restraining ring is 1.5 m.

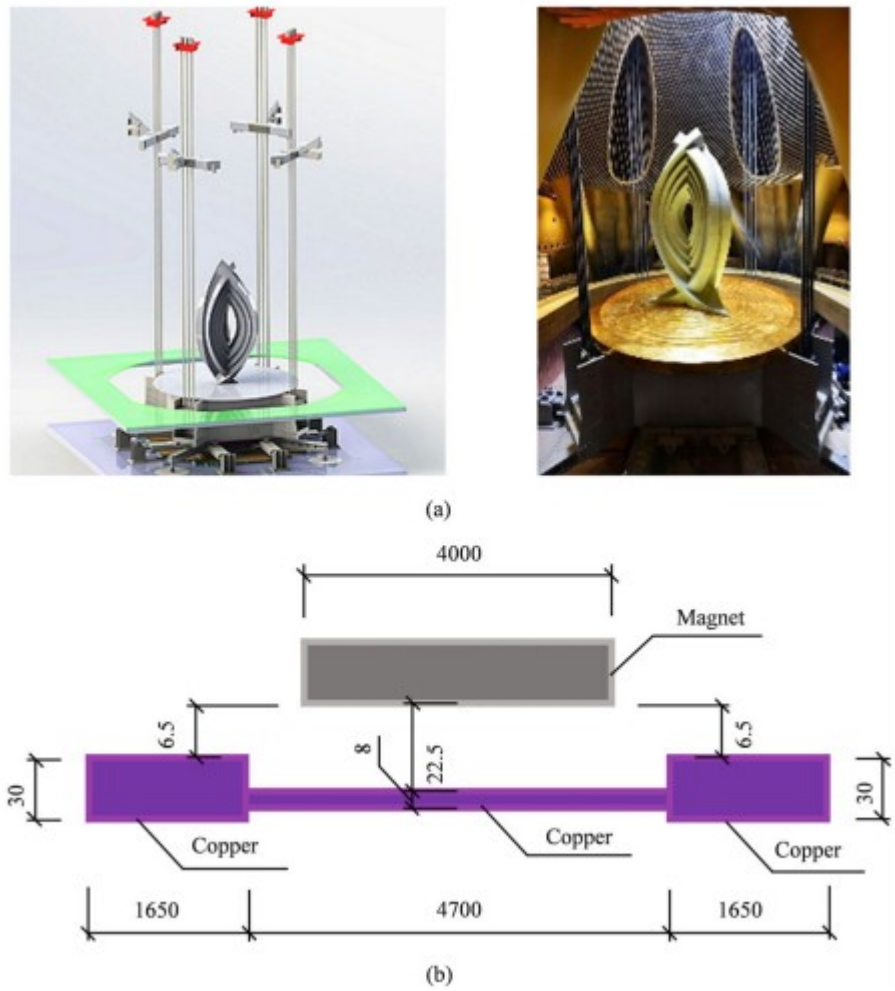

Figure 2

Illustration of the eddy-current TMD (a) and the relative location of the magnet plate and the copper plate (b). TMD = tuned mass damper

It is necessary to control the displacement of TMD to be within the above ranges of displacements under a strong wind or earthquake loading. The main aim of using the eddy-current TMD is to generate variable damping ratio under different displacements: low damping ratio under a moderate displacement and high damping ratio under a large displacement. This aim can be achieved by two means: (a) selecting and arranging of the number of permanent magnets and (b) controlling the distance between the permanent magnet and the conductor.

The damping system of the eddy-current TMD is installed underneath the mass block. At the bottom of the mass block, 1,800 pieces of permanent magnets are arranged as a disk with a diameter of 4 m. A nonuniform thick copper plate with a diameter of 8 m is firmly attached to the 125th floor under the restraining ring. Figure 2(b) shows the dimension of the copper plate and the magnets. The central part of the copper, with a diameter of 4.7 m, has a thickness of 8 mm. The outside part is 30 mm thick and has a form

of an annular disk, with the inner and outer diameter of 4.7 and 8 m, respectively. Copper plate is located 22.5 and 6.5 mm away from the magnet for the central part and for the outside part of the copper plate, respectively. The on-site photo of the TMD in SHT is shown on Figure 2(a).

The minimum and maximum damping ratio of the eddy-current TMD can be calculated.[22]The correlation between the damping ratio of the TMD and the displacement is illustrated in Figure 3. The displacement value of 0.35 m presents a difference between the radius of the central part of the copper plate and the magnet. This displacement refers to the displacement at which the magnet begins to cross over the thicker and outside part of the copper plate. A displacement value of 1.5 m is where the snubber would touch the restraining ring and viscous dampers.

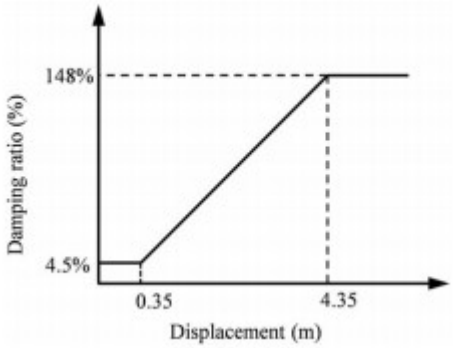

Figure 3

Damping ratio of the eddy-current tuned mass damper with displacement

3.2 Simulation of the eddy-current TMD

The main parameters of the eddy-current TMD in SHT are shown in Table 1. The TMD's behavior can be modeled by using Pendulum Theory. A simple pendulum model is displayed in Figure 4. Because the length of rope is much longer than TMD motion, it can be assumed that the pendulum angle θ is small and that the resisting force and the magnetic force are horizontal. In that case, the resistance stiffness k_h and the axial stiffness k_v can be calculated from Equations 1 and 2, respectively.

$k_h = G/l$, (1)

$k_v = EA/l$, (2)

TABLE 1 Parameters of the eddy-current TMD in SHT

Main parameters	Value or formula	Unit
Target frequency	0.111	Hz
TMD mass	1,000	Ton
TMD mass to structural generalized mass ratio	0.96	%
Cable length (based on target frequency)	20.6	m
Magnetic force	$F_{magnetic} = C_{magnetic}*V$ (C is given in Figure 3)	/
Protection devices (viscous dampers)	$F_{SVDD} = C_{snubberVDD}*V^{0.2}$; $C_{snubberVDD}$ = 1,100 kN/(m/s)$^{0.2}$	/
Maximum impact force against protective ring	8,000	kN

Note. SHT = Shanghai Tower; TMD = tuned mass damper.

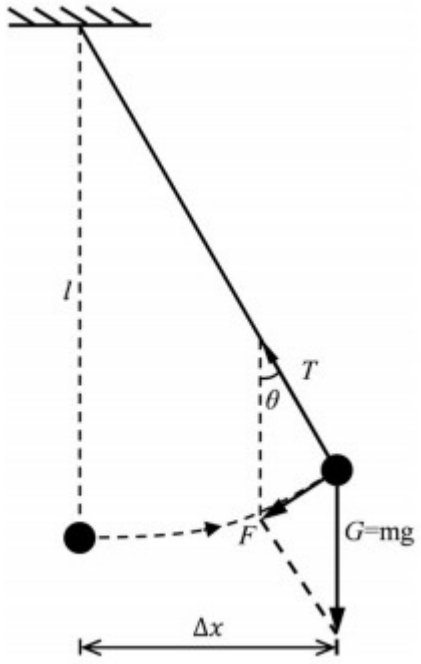

Figure 4

Diagram of single pendulum

where G is the gravity of the TMD, l is the length of the ropes, E is the elastic modulus, and $A$is the section area of the ropes.

The damping coefficient c is calculated from Equation 3:

$$c(\Delta x) = 4\pi m f \cdot \zeta(\Delta x), \quad (3)$$

where ζ is the damping ratio, Δx is the displacement, m is the mass, and f is the frequency of the TMD.

The stiffness k_h and k_v are displacement-independent, whereas the damping coefficient c is displacement-dependent. In order to properly model the mechanical behavior of the TMD, four CONNECTOR elements in ABAQUS are used to model the four sets of cables. Each CONNECTOR element connects two nodes, that is, two ends of one set of cables, and is defined by three translational stiffness in three coordinate directions and two translational displacement-dependent damping coefficient in two horizontal coordinate

directions. The displacement-dependent damping coefficient is defined in ABAQUS by CONNECTOR element through three data sets: damping forces, velocity, and relative displacement, as illustrated in Table 2. By assuming large velocity limits (−100 and 100 m/s) at different relative displacement values, all possible magnetic forces can be considered.

TABLE 2 Definition of the displacement-dependent damping coefficient in ABAQUS

Damping forces (kN)	Velocity (m/s)	Relative displacement (m)
−51,610.08	−100	−10
51,610.08	100	−10
−51,610.08	−100	−4.35
51,610.08	100	−4.35
−1,551.89	−100	−0.35
1,551.89	100	−0.35
−1,551.89	−100	0.35
1,551.89	100	0.35
−51,610.08	−100	4.35
51,610.08	100	4.35
−51,610.08	−100	10
51,610.08	100	10

Detailed information of eight viscous dampers is shown in Table 1. Different from the TMD magnetic force, the damping force of the viscous dampers is proportional to $v^{0.2}$. This is a regular viscous damper and can be modeled by DASHPOT element or CONNECTOR element in ABAQUS.

3.3 Verification of modeling method of TMD

To verify that the TMD can be properly simulated, it is first necessary to develop a stand-alone TMD model that is not embedded in SHT model. The mass block with four sets of cables is simulated in ABAQUS in advance. A static gravity analysis step is followed by a natural frequency analysis step. The first three modes are shown in Figure 5. The first two modes are translation mode, and the third mode is a torsional mode. The first natural frequency, 0.110 Hz, is very close to the design value of the TMD in SHT illustrated in Table 1. In the following section, it will be shown that the displacement-dependent damping coefficient and the resisting stiffness can also be properly modeled.

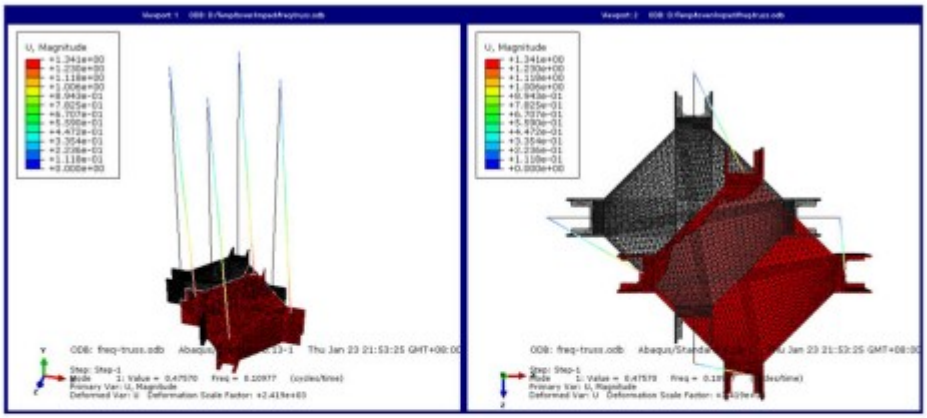

(a) First modal shape

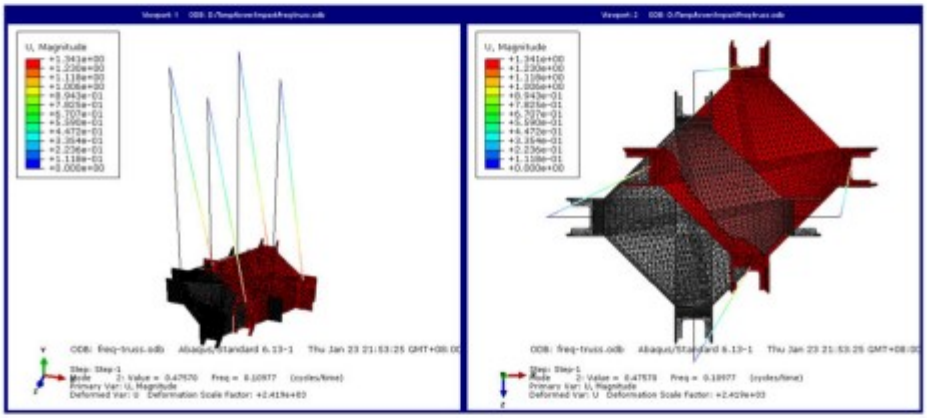

(b) Second modal shape

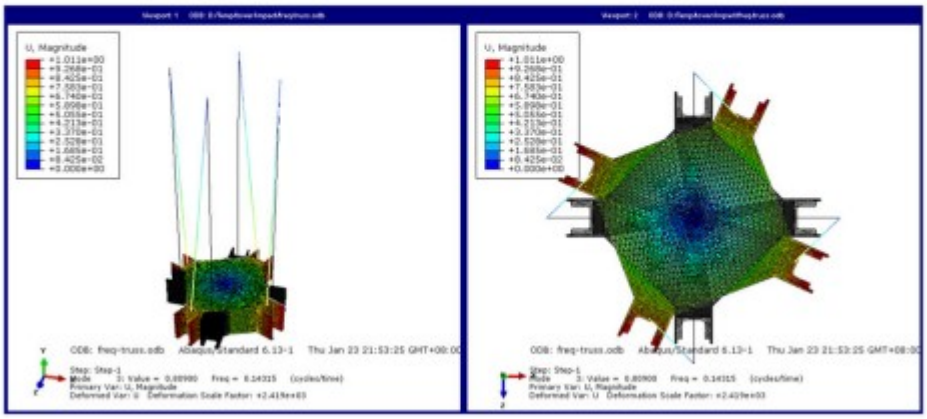

(c) Third modal shape

Figure 5

First three modal shapes of the tuned mass damper

4 NUMERICAL SIMULATION OF THE SHT

4.1 Finite element model of the SHT

A SHT model without TMD was set up by Jiang et al.[23] in ABAQUS. In this study, the eddy-current TMD mass body and the protection devices are

added to the SHT model. This is done using solid elements, shell elements, CONNECTOR elements, and contact option, as illustrated in Figure 6. The mega-columns, the shear walls, and the coupling beams in the core tube are simulated using the multilayer shell elements. The inner shape steels are simulated using beam elements, which are connected to the shell model by sharing nodes. The steel frame, outrigger, and steel tower at the top are simulated by beam elements. It is assumed that the building is linear, and the TMD is nonlinear.

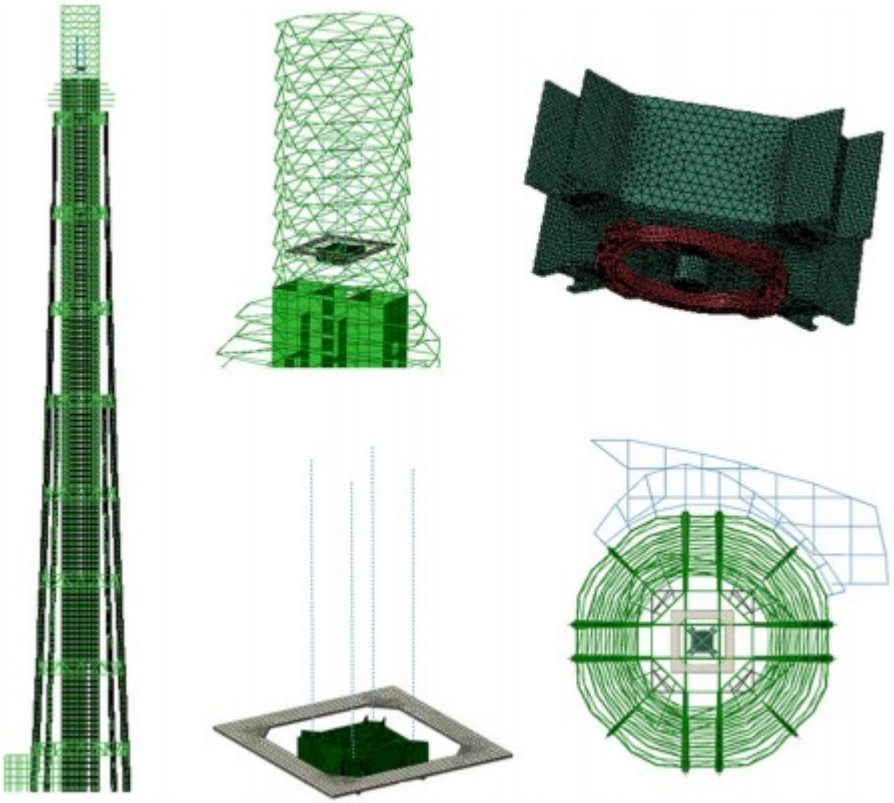

Figure 6

Finite element model of Shanghai Tower in ABAQUS

Two finite element SHT models were prepared. For one model, it is assumed that the bottom is fixed, whereas the other model considers SSI effect. Because the depth of embedment of the foundation is much smaller than the total height of SHT, this study will focus on the influence of the rotation of the soil-foundation system on the structure responses under wind and earthquake excitations.[21] Hence, the horizontal and vertical movements of the soil-foundation system are ignored. Therefore, the soil-foundation system of SHT is simplified to a series of linear rotation springs at the bottom of the structure. Li et al.[21] calculated the rotational stiffness, K, to be approximately 4.36×10^{13} N•m/rad by using a refined finite element model of the foundation and adjacent soil. This value of K is used in this study. Schematic illustration of analytical methods of the SSI under wind load and earthquake is shown in Figure 7.

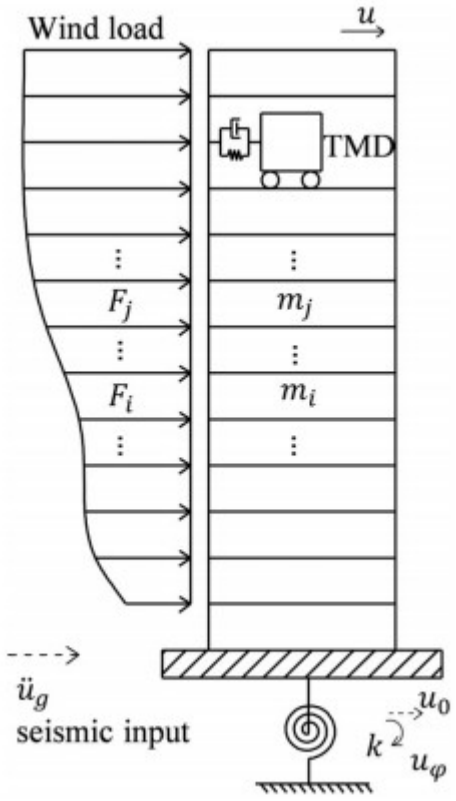

Figure 7

Schematic illustration of analytical methods of the soil-structure interaction. TMD = tuned mass damper

4.2 Structural dynamic properties

The Rayleigh damping is used for the SHT model. The damping ratio is assumed to be 1% for wind load analyses and 5% for seismic analyses to consider the expected nonlinear behavior under rare earthquakes. Modal analyses of the SHT model with and without SSI are conducted using the Lanczos method. Table 3 shows the dynamic properties of the structure with and without SSI effects. The natural frequency of SHT is approximately 0.106 Hz without SSI effects and 0.088 Hz with SSI effects. The value 0.106 Hz is a little different from the value 0.110 Hz described in Section 3.3, as 0.110 Hz is from the analysis of a different model, that is, the stand-alone TMD model. After considering SSI effects, the frequency of SHT is obviously decreased; thus, the period of the TMD becomes different from that of the SHT. It is noted that the frequency of torsional mode remains almost constant even with SSI effects.

TABLE 3 Structural dynamic properties with and without SSI effects

Mode	Frequency with SSI effects (Hz)	Remarks	Frequency without SSI effects (Hz)	Remarks
1	0.088	First translation in the Y direction	0.106	First translation in the Y direction
2	0.092	First translation in the X direction	0.108	First translation in the X direction
3	0.112	Second translation in the Y direction	0.118	Second translation in the Y direction
4	0.112	Second translation in the X direction	0.123	Second translation in the X direction
5	0.300	Third translation in the Y direction	0.306	First torsion
6	0.305	First torsion	0.317	Third translation in the Y direction
7	0.308	Third translation in the X direction	0.322	Third translation in the X direction
8	0.617	Second torsion	0.617	Second torsion
9	0.657	Fourth translation in the Y direction	0.676	Fourth translation in the Y direction
10	0.660	Fourth translation in the X direction	0.677	Fourth translation in the X direction

Note. SSI = soil-structure interaction.

4.3 Analysis of wind-induced response

For the wind loading behavior analyses, time history wind force records were considered for two wind angles (80° and 270°). These two wind load directions represent two most unfavorable directions, as identified from the wind tunnel tests by Rowan, Williams, Davies & Irwin, Inc. Recorded time histories of wind loads in given directions were used as excitation for the wind load analyses of the structure. The maximum wind speed, duration, and the corresponding maximum force on TMD floor are listed in Table 4. Time history wind forces were simultaneously applied at each floor in the X and Y directions of the building. For example, Figure 8 shows the wind force time-history corresponding to the TMD floor for a 100-year return period for wind at angles of 80° and 270°. It can be seen from this figure that the wind forces are composed of the average wind force and the fluctuating wind force.

TABLE 4 Information of wind loads

Return period (year)	Maximum wind speed (m/s)	Maximum wind force on TMD floor (kN)	Duration (s)
1	26.59	110.95	8,291.19
10	37.84	228.84	5,823.77
50	47.18	351.80	4,292.61
100	50.66	404.99	4,373.58

Note. TMD = tuned mass damper.

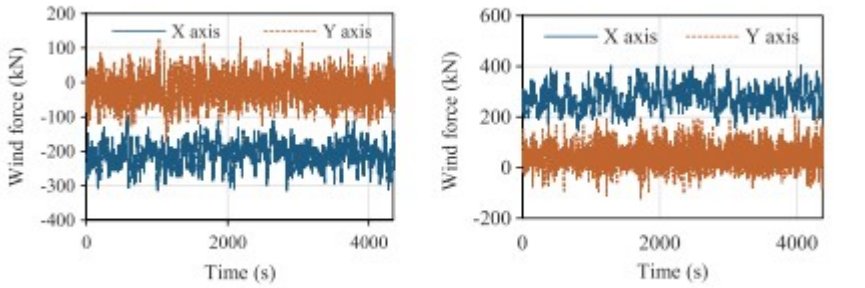

(a) 100-year return period with wind angle 80° (b) 100-year return period with wind angle 270°

Figure 8

Time history wind force curves on tuned mass damper floor

Analytical results of the wind-induced response with and without SSI effects in ABAQUS model are shown in Tables 5, 6, and 7. Tables 5 and 6 show the acceleration and displacement responses of the building. It can be observed that the structural response for wind loads at angle 80° is smaller than that for wind loads at angle 270°, for long return period wind hazards. Herein, statistical peak value, x, is calculated by the following equation:

$$x = 2.5\times\sqrt{\frac{\sum_{i=1}^{n} x_i^2}{n}}, (i = 0, 1, ..., n),$$

TABLE 5 Statistical peak values of acceleration responses in wind analyses (m/s^2)

Return period (year)	Floor	Wind direction A = 80°			Wind direction A = 270°		
		With SSI	Without SSI	Difference (%)	With SSI	Without SSI	Difference (%)
1	Top	0.075	0.033	127.27	0.054	0.028	92.86
	TMD floor	0.067	0.029	131.03	0.049	0.025	96.00
10	Top	0.197	0.118	66.95	0.281	0.137	105.11
	TMD floor	0.177	0.104	70.19	0.253	0.121	109.09
50	Top	0.223	0.229	−2.62	0.284	0.356	−20.22
	TMD floor	0.2	0.203	−1.48	0.256	0.318	−19.50
100	Top	0.247	0.24	2.92	0.296	0.407	−27.27
	TMD floor	0.221	0.213	3.76	0.266	0.365	−27.12

Note. SSI = soil-structure interaction; TMD = tuned mass damper; Underlined values mean exceeding design limits of human comfort.

TABLE 6 Statistical peak values of displacement responses in wind analyses (m)

Return period (year)	Floor	Wind direction A = 80°			Wind direction A = 270°		
		With SSI	Without SSI	Difference (%)	With SSI	Without SSI	Difference (%)
1	Top	0.339	0.2	69.50	0.411	0.226	81.86
	TMD floor	0.302	0.175	72.57	0.364	0.194	87.63
10	Top	0.806	0.433	86.14	1.155	0.528	118.75
	TMD floor	0.721	0.377	91.25	1.032	0.457	125.82
50	Top	1.055	0.704	49.86	1.396	0.982	42.16
	TMD floor	0.94	0.614	53.09	1.241	0.857	44.81
100	Top	1.191	0.774	53.88	1.537	1.122	36.99
	TMD floor	1.06	0.674	57.27	1.365	0.979	39.43

Note. SSI = soil-structure interaction; TMD = tuned mass damper.

TABLE 7 TMD amplitude in wind analyses (m)

Return period (year)	Direction	Wind direction A = 80°			Wind direction A = 270°		
		With SSI	Without SSI	Difference (%)	With SSI	Without SSI	Difference (%)
1	X	0.283	0.302	−6.29	0.282	0.319	−11.60
	Y	0.502	0.530	−5.28	0.363	0.459	−20.92
10	X	0.627	0.678	−7.52	0.480	0.475	1.05
	Y	1.055	1.175	−10.21	1.415	1.416	−0.07
50	X	0.802	0.927	−13.48	0.840	0.904	−7.08
	Y	1.199	1.457	−17.71	1.449	1.534	−5.54
100	X	0.860	0.956	−10.04	0.878	0.956	−8.16
	Y	1.204	1.521	−20.84	1.394	1.529	−8.83

Note. SSI = soil-structure interaction; TMD = tuned mass damper.

where x_i is the acceleration or displacement value at the ith increment of the time history. The 2.5 stands for peak factor, which is the ratio of max value and root mean square value.

As demonstrated in Table 5, SSI has a more significant effect on acceleration response for wind loads with a short return period (1- and 10-year) than wind loads with a long return period (50- and 100-year). As the underlined numbers shown in Table 5, some of the acceleration responses with SSI effects exceed design limits of human comfort, that is, 0.036 and 0.25 m/s^2 for wind loads with 1- and 10-year return period, respectively. Average relative differences between cases with SSI effects and cases without SSI effects are 112%, 88%, −11%, and −12% for 1-, 10-, 50-, and 100-year return period wind load, respectively. Herein, relative difference is the response with SSI subtracts that without SSI, divided by the response without SSI. Positive percentage means the response with SSI is bigger. As illustrated in Table 6, displacement response increases after considering SSI effects. Average relative differences of displacement response between cases with SSI and cases without SSI are approximately 78%, 105%, 47% and 47% for 1-, 10-, 50-, and 100-year return period wind load, respectively. Increase of displacement response due to SSI can be attributed to the fact that the natural period is extended after considering SSI and that the wind is a long period dominant load. In addition, structural system with SSI effects becomes softer, thus allowing more displacements.

Table 7 lists the analytical predictions of the TMD displacement amplitude. It is clear that SSI reduces the TMD displacement amplitudes for all the wind sequences except for the one having 10-year return period with wind angle 270°. For this wind load, with 10-year return period at an angle of 270°, analysis with SSI shows very limited effect on the TMD displacement amplitude. For the wind sequences causing impacts between the TMD and the restraining ring, Figure 9 shows the histories of the impact force and the TMD displacement relative to the restraining ring with and without SSI effects. The results show that impacts would happen under wind sequences with 50-year (only for wind angle 270°) and 100-year return periods when the SSI effect is not considered, and under wind sequence with 50-year return period with wind angle 270° when the SSI effect is considered. Impact can amplify the acceleration response. Taking the wind sequence with a 100-year return period and with wind angle 270° as an example, Figure 10 shows the acceleration and the displacement response histories on the TMD floor and the top of the SHT. It can be seen that the wind loads with angle 270° features more frequent impact loads than wind loads with angle 80°. It is also noted that impact is almost nonexistent for model with SSI effect. The maximum impact force is 4,168 kN, which is less than 8,000 kN, representing the strength capacity of the protection ring. In these analyses, the TMD displacement relative to the 125th floor remains less than 2 m, which means the protective ring or mass block would not impact the main structure.

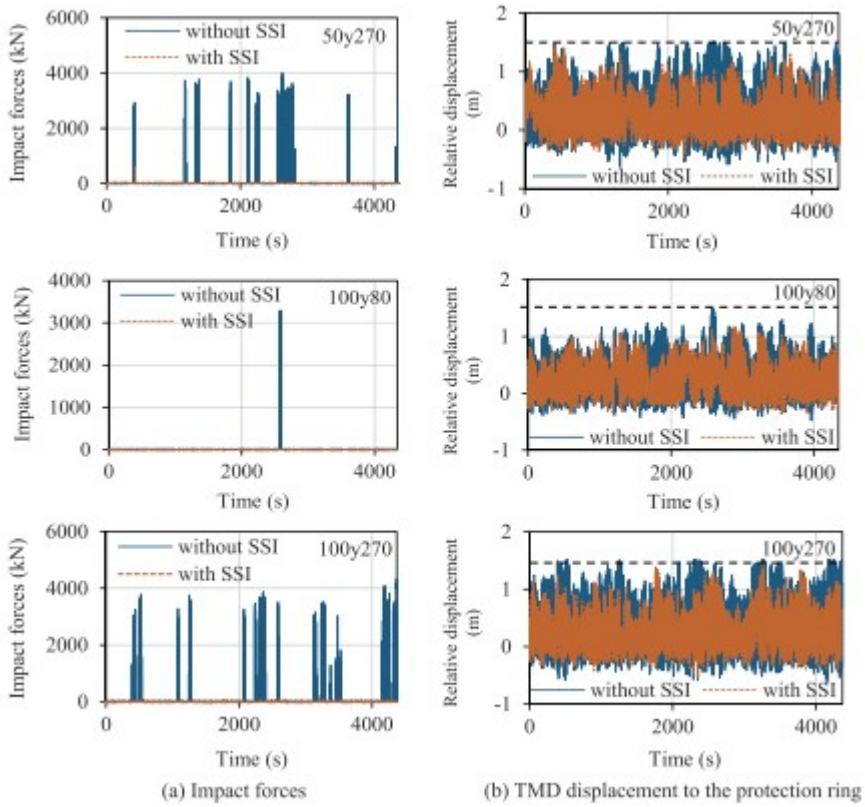

Figure 9

Impact forces (a) and relative displacement (b) between the TMD and the protection ring under wind load. TMD = tuned mass damper

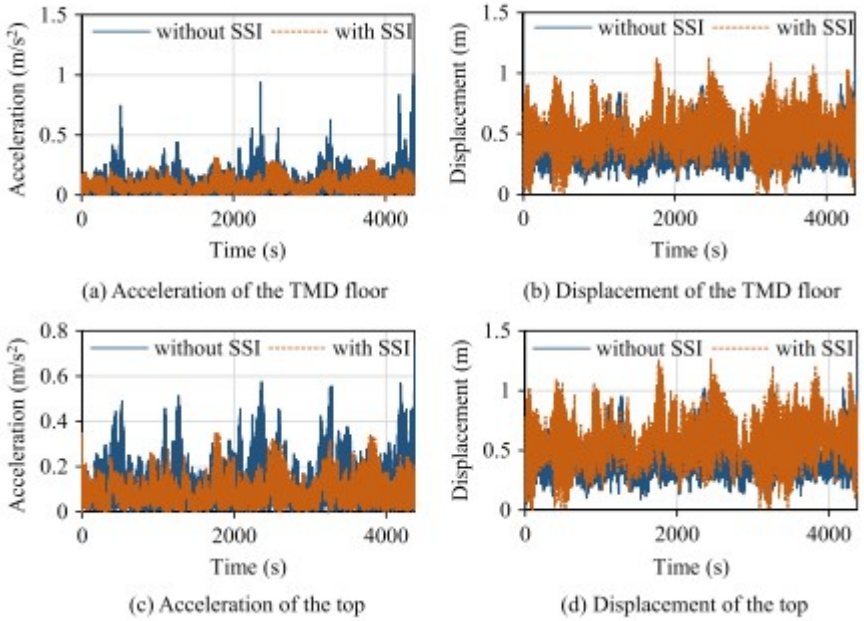

Figure 10

Responses of the TMD floor and the top under 100-year/angle 270° wind load with and without SSI effects. SSI = soil-structure interaction; TMD = tuned mass damper

Horizontal displacement envelopes of different floors under various return period wind loads are shown in Figure 11. When SSI is not considered, the displacement envelope shows limited differences for two wind angles for wind loads with a short return period, whereas differences are more significant for wind loads with longer return periods. When SSI is considered, the displacement envelope shows differences for two wind angles. In addition, displacement envelope features larger values than that without SSI for all considered wind loads. This is consistent with the results in Table 6.

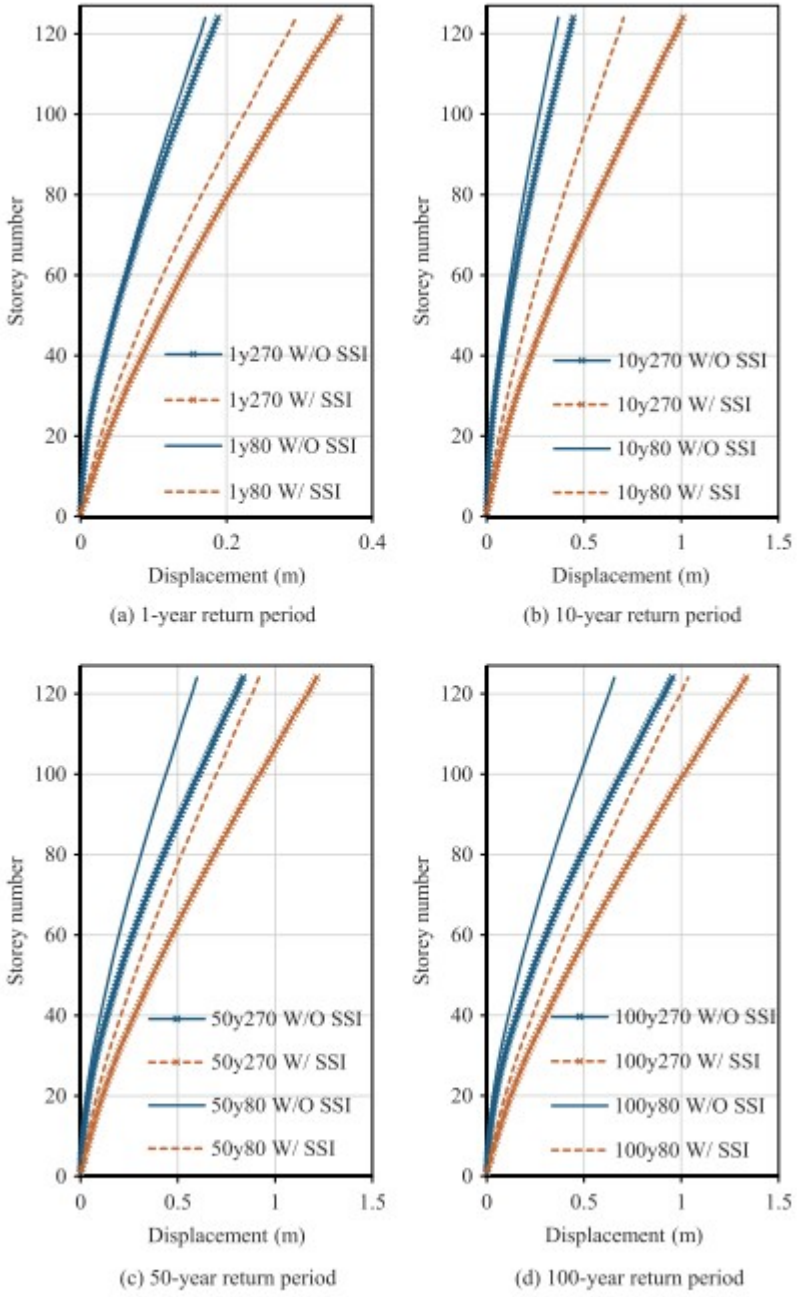

Figure 11

Displacement envelope curves under wind loads

4.4 Analysis of seismic-induced response

For the seismic analyses, two synthesized and five recorded two-horizontal-component ground motions were used as rare earthquake excitations. Chosen seismic motions are in compliance with the *Code for Seismic Design of Buildings*.[24] The effective duration of each motion, which is defined as the duration from the time the acceleration reaches 10% of peak ground acceleration (PGA) to the time the acceleration becomes less than 10% of PGA, is no less than five times of the natural period of the building, calculated and presented earlier as 9.43 s. The acceleration time history response spectra of the NRXY3 record (the X component and Y component of NRXY3) are shown in Figure 12. The ground motions were imposed on the building with or/and without SSI effects, along both the X and Y directions, with the PGA of 0.2 and 0.17 g, respectively.

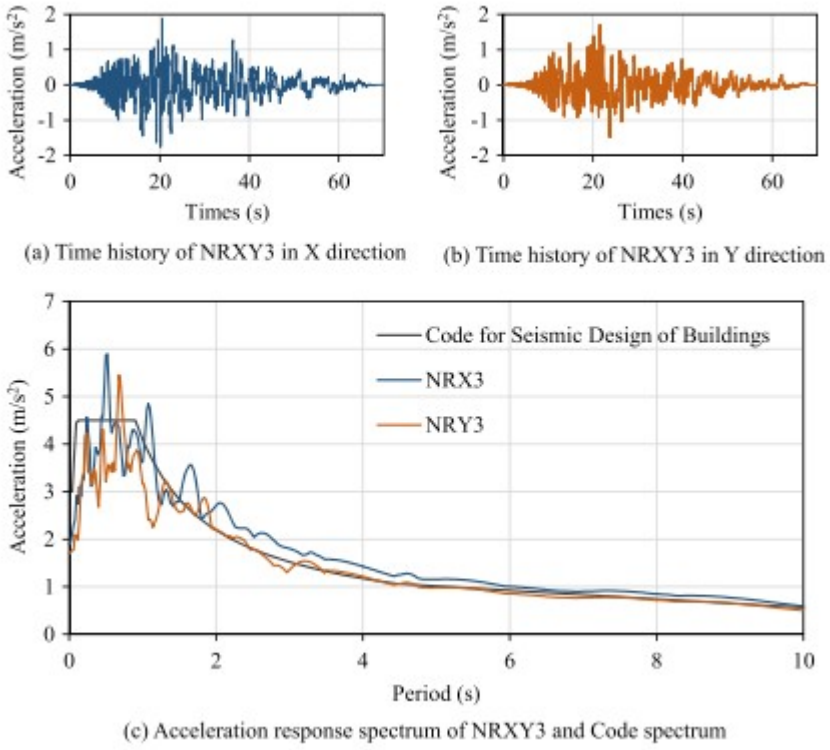

Figure 12

Acceleration time history and response spectrum of the NRXY3 wave

The analytical results for the seismic response analyses are shown in Table 8. It can be concluded that, by taking into account the SSI effects, all the indices shown in the table decrease. The natural period of the building without SSI is 9.43 s. SSI effects extended the natural period of the building to 11.31 s; thus, the period of the TMD becomes different from that of the building. Therefore, the response values of the TMD shown in Table 8 were

decreased after considering SSI effects. Table 8 shows that under the seven ground motions, the average value of the maximum impact force without and with SSI effect is 6,809 and 6,475 kN, respectively. It is noted that this value is larger than that obtained from the wind load analyses; however, it still does meet the design limit of 8,000 kN. Table 8 indicates that for the two set of records, the protective ring impacts the structure.

TABLE 8 Summary of seismic results with SSI and without SSI

	TMD displacement to the TMD floor (m)		Maximum TMD amplitude to hang point (m)		Maximum eddy-current damping force (kN)		Maximum impact force (kN)	
Sequence	With SSI	Without SSI	With SSI	Without SSI	With SSI	Without SSI	With SSI	Without SSI
AWX1 + 0.85AWY1	1.82	1.89	1.71	1.80	1,214	1,273	6,546	6,826
AWX2 + 0.85AWY2	1.82	1.86	1.75	1.83	1,420	1,473	6,083	6,364
NRX3 + 0.85NRY3	1.84	2.17	1.82	2.11	1,310	1,703	6,785	7,285
NRX4 + 0.85NRY4	1.75	1.82	1.70	1.80	1,088	1,347	6,211	6,968
NRX5 + 0.85NRY5	1.80	2.20	1.75	2.07	941	1,147	6,654	6,757
NRX6 + 0.85NRY6	1.85	1.97	1.75	1.88	1,059	1,208	6,431	6,647
NRX7 + 0.85NRY7	1.76	1.88	1.70	1.78	1,110	1,245	6,613	6,815
Average value	1.81	1.97	1.74	1.89	1,163	1,342	6,475	6,809

Note. SSI = soil-structure interaction; TMD = tuned mass damper.

The averaged displacement envelops and the averaged story drift ratios of the SHT under seven input motions are shown in Figure 13. Because the PGA of the input motions in X direction is larger than that in Y direction, the response displacement in X direction is greater than that in Y direction. After considering the SSI effects, the displacement in X direction is increased slightly whereas the displacement in Y direction is decreased for the upper part of the building. However, the story drift ratio shows different trends. SSI effect increases the story drift ratio for the lower part of the building while decreases the story drift ratio for the upper part of the building.

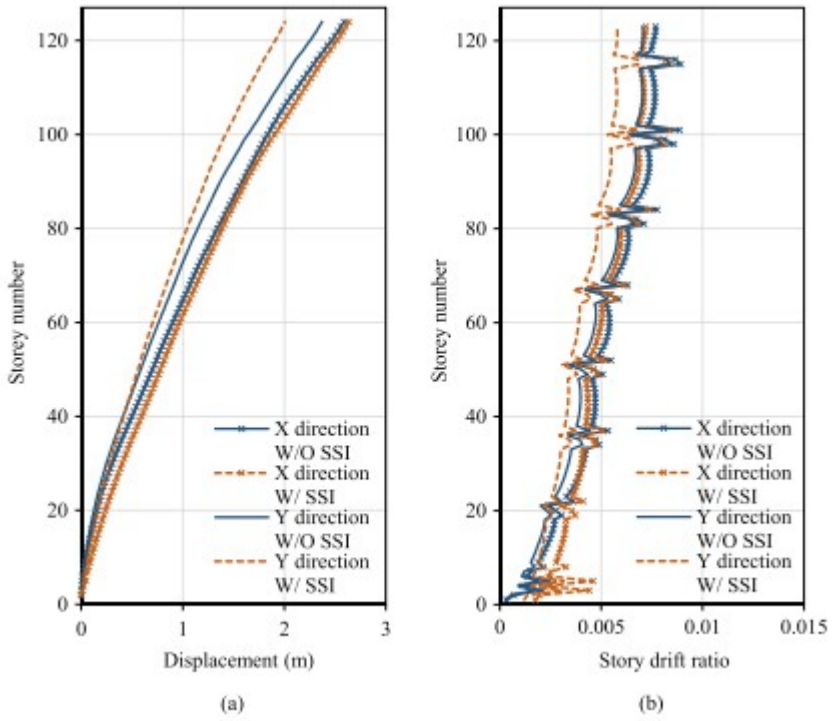

Figure 13

Averaged values of seven waves: (a) displacement envelope curve and (b) story drift ratio. SSI = soil-structure interaction

Figure 14 shows the impact forces and the relative displacement of the TMD and the TMD floor for the NRXY3 motion. In variance to the effect of SSI on the maximum impact force under wind loads, the SSI effect on the maximum impact force under the seven ground motions is smaller. The average relative difference of the maximum impact force is 4.9%. The SSI effect reduces the displacement between the TMD and the TMD floor, with the average relative difference of 8.1%.

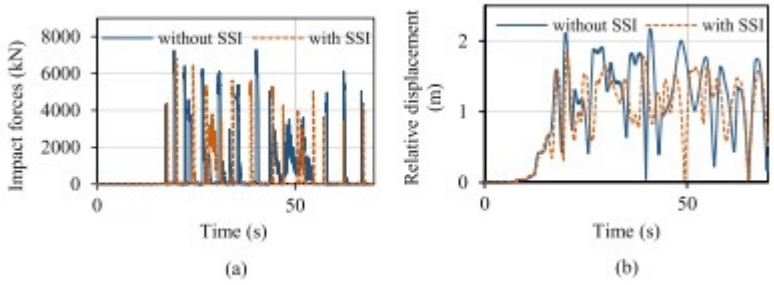

Figure 14

Impact forces (a) and relative displacement between TMD and TMD-floor (b) of case that excited by NRXY3. SSI = soil-structure interaction; TMD = tuned mass damper

Figure 15(a) shows the relative displacement and the damping coefficient curves resulting from the NRXY3 motion, as well as the defined theoretical

curve for the CONNECTOR elements. It can be seen that the numerical results agree very well with theoretical values. The relative displacement and the connector viscous force correlation curves excited by the NRXY3 motion are illustrated in Figure 15(b). The area enclosed by the curve represents the damping energy dissipation. It is clear that when the relative displacement is larger than 0.35 m, the viscous force and the area increase significantly, which results in the TMD dissipating more energy at large amplitude.

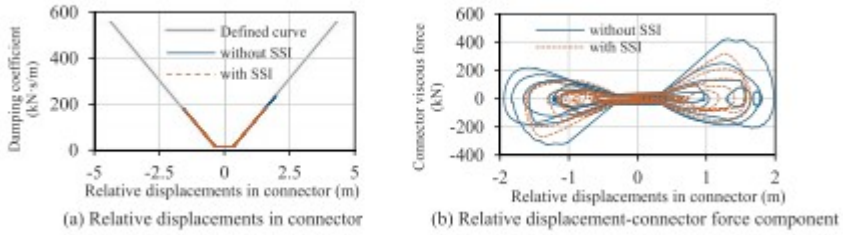

Figure 15

Displacement-damping coefficient (a) and displacement-connector viscous force component (b) of one rope excited by NRXY3. SSI = soil-structure interaction

5 CONCLUSION

SHT is a super high-rise building in China. A new eddy-current TMD was installed in the building to mitigate structural vibrations due to wind and earthquake excitations. This paper proposes a method to simulate the new eddy-current TMD whose damping ratio is displacement-dependent. The influence of SSI on performance of the SHT is also studied. The following conclusions can be drawn:

1. The proposed method to simulate the new eddy-current TMD can be used to properly model the displacement-dependent damping behavior. It can be used for both wind and seismic loading analyses of buildings with this kind of eddy-current TMD.

2. Impact elements can be embedded into the complete, detailed structural model to perform dynamic analyses of buildings with TMD. Although this type of sophisticated analysis adds computational time, it is recommended to perform this type of high fidelity, detailed dynamic analyses in order to study the performance of the systems.

3. For wind loading induced responses, SSI effects have a more significant effect on acceleration response for wind loads with a shorter return period (1- and 10-year) than that with a longer return period (50- and 100-year). Some of the acceleration responses with SSI effects exceed design limits of human comfort for wind loads with shorter return periods. Thus, it is necessary to consider SSI effects from the point view of human comfort design. Average relative differences of acceleration response between cases with SSI effects and cases without SSI effects are 112%, 88%, −11%, and −12% for 1-, 10-, 50-, and 100-year return period wind loads, respectively. Average relative differences of displacement response between cases with

SSI and cases without SSI are 78%, 105%, 47%, and 47% for 1-, 10-, 50-, and 100-year return period wind loads, respectively. SSI effects reduce the TMD displacement amplitudes for all the wind load cases except for the one with 10-year return period with wind angle 270°. For this case, inclusion of SSI effects shows very limited effect on the TMD displacement amplitude. Thus, SSI effects reduce the amplitude of impact between the TMD and the protection ring. The maximum impact force under 100-year return period wind loads is less than the strength capacity of the protection ring. For none of the analyzed cases, the TMD and the protective ring would impact the main structure.

4. For dynamic responses under a rare earthquake that matches the design code, SSI effects slightly reduce the displacement amplitude, the damping force, and the impact force of the TMD. SSI effects increase the story drift ratio for the lower part of the building while decrease the story drift ratio for the upper part of the building.

5. From the above discussions, it is clear that it is necessary to consider SSI effects for high-rise buildings on soft soils.

ACKNOWLEDGEMENTS

The authors wish to gratefully acknowledge the support of this work by the collaborative research project under International Joint Research Laboratory of Earthquake Engineering (ILEE) under Grant ILEE-IJRP-P1-P3-2016, the Natural Science Foundation of China under Grants 51478357 and 51778491, and the National Science & Technology Pillar Program of China under Grant 2015BAK17B04.

Biographies

- Zhiguang Zhou is an associate professor of the College of Civil Engineering, Tongji University. His research interests are response control and seismic isolation of buildings and seismic performance of power energy structures.
- Xiaodong Wei is a graduate student of Tongji University in China. His research focuses on response control and seismic isolation of buildings.
- Zheng Lu is a professor of the College of Civil Engineering, Tongji University. His research interests are structural control and earthquake engineering.
- Boris Jeremic is a professor of the Department of Civil and Environmental Engineering, University of California, Davis. His research interests lie in static and dynamic, deterministic and probabilistic modeling, and simulation of inelastic solids and structures.

REFERENCES

[1] H. Frahm, 1909, US Patent 0989958. [2] G. W. Housner, L. A. Bergman, T. K. Caughey, J. Eng. Mech. 1997, 123(9), 897. [3] F. Sadek, B. Mohraz, A.W.

Taylor, R.M. Chung, US Department of Commerce, National Institute of standards and Technology, 1996. [4] X. L. Lu, Q. Zhang, D. G. Weng, Z. G. Zhou, Struct. Control Health Monit. 2016, 24(3), 1882. [5] D. C. Giancoli, Physics: Principles with Applications, 5th ed., Prentice Hall, Upper Saddle River, NJ 1998. [6] F. T. Ulaby, E. Michielssen, U. Ravaioli, Fundamentals of Applied Electromagnetics, 5th ed., Prentice Hall, Upper Saddle River: NJ 2007. [7] ASCE, 7–10Minimum Design Loads for Buildings and Other Structures, American Society of Civil Engineers/Structural Engineering Institute, USA 2010. [8] J. F. Wang, C. C. Lin, Int. J. Solids Struct. 2005, 42(20), 5536. [9] J. Wu, G. Chen, M. Lou, Earthquake Eng. Struct. Dyn. 1999, 28(11), 1219. [10] J. P. Wolf, Foundation vibration analysis using simple physical models, 1st ed., PTR Prentice Hall, Englewood Cliffs 1994. [11] C. T. Chatzigogos, A. Pecker, J. Salencon, Soil Dyn. Earthq. Eng. 2009, 29, 765. [12] M. Moghaddasi, M. Cubrinovski, J. G. Chase, Eng. Struct. 2011, 33, 1338. [13] M. Moghaddasi, M. Cubrinovski, J. G. Chase, Eng. Struct. 2011, 40, 135. [14] M. Moghaddasi, G. A. MacRae, J. G. Chase, Eng. Struct. 2015, 44, 1805. [15] W. L. Finn, B. H. Pandey, C. E. Ventura, Struct. Design Tall Spec. Build. 2011, 20, 47. [16] I. Venanzi, D. Salciarini, C. Tamagnini, Eng. Struct. 2014, 79, 117. [17] R. Chen, J Vib Shock 1999, 18(2), 10. [18] R. Chen, Chin. J. Rock Mech. Eng. 2003, 22(2), 309. [19] C. X. Fan, R. Chen, Chin. J. Rock Mech. Eng. 2004, 23(12), 2078. [20] M. Y. Liu, J. Wind Eng. Ind. Aerodyn. 2008, 96, 1092. [21] M.K. Li, X. Lu, X.Z. Lu, J. Rock Mech. Geotech. Eng., 2014, 6, 477. [22] R. Zemp, J. C. Llera, J. L. Almazán, Earthquake Eng. Struct. Dyn. 2011, 40, 339. [23] H. J. Jiang, L. S. He, X. L. Lu, J Building Struct 2011, 32(11), 55. [24] DGJ08–9-2013, Code for seismic design of buildings, Ministry of Housing and Urban-Rural Development of Shanghai, China 2013.